Tribology International 43 (2010) 868–875

Contents lists available at ScienceDirect

Tribology International

journal homepage: www.elsevier.com/locate/triboint

Corrosion wear behaviors of micro-arc oxidation coating of Al_2O_3 on 2024Al in different aqueous environments at fretting contact

Hong-yan Ding [a,*], Zhen-dong Dai [b], Suresh C. Skuiry [c], David Hui [d]

[a] Faculty of Mechanical Engineering, Huaiyin Institute of Technology, Huaian 223003, China
[b] Academy of Frontier Science, Nanjing University of Aeronautics and Astronautics, Nanjing 210016, China
[c] Center for Tribology, Inc., Campbell 95008, CA, USA
[d] Department of Mechanical Engineering, University of New Orleans, New Orleans 70148, LA, USA

ARTICLE INFO

Available online 22 December 2009

Keywords:
micro-arc oxidation
Artificial seawater
Artificial rainwater
Corrosion wear

ABSTRACT

The fretting wear behavior of micro-arc oxidation (MAO) coating of Al_2O_3 on an aluminum alloy 2024Al flat against a 440C stainless steel ball was investigated in artificial rainwater, artificial seawater and distilled water by using a ball-on-flat configuration with 300 μm amplitude at room temperature for 1 h. The morphology of the wear scars were observed and analyzed using scanning electron microscopy; the 3D-morphology and wear volume-loss were determined using a non-contact optical profilometer. Potentiodynamic anodic polarization was used to measure the corrosion behavior of the MAO coating before and after the corrosion wear test. The influences of the load, frequency and aqueous medium on the friction coefficient and wear volume-loss of the coatings were also analyzed. Results show that the friction coefficient decreases generally with an increase of the frequency in the three aqueous solutions; whereas it presents different variation trends as the load increased. In addition, aqueous environment does significantly influence the friction coefficient, the friction coefficient was the largest when fretting occurred in distilled water, smaller when fretting occurred in rainwater, and the smallest when fretting occurred in seawater. Particularly the remarkable antifriction effect of the seawater is of note. The wear-loss of the MAO coating in the distilled water is the largest at low frequency; however, it increases rapidly in rainwater and seawater at high frequency due to the corrosion effect of Cl^- ion as well as its accelerating effect to the wear process, and results in larger wear-loss than that in distilled water, which implies a positive synergism between corrosion and wear.

1. Introduction

Aluminum alloys as weight-saving materials are becoming increasingly important, both in the automotive and aerospace industries. However, as far as the tribological machine parts are concerned, the poor wear-resistance of aluminum alloys decreases the service life of machine components especially in corrosive environments [1–3]. Therefore, to enhance their wear-resistance, a number of techniques have been investigated to produce ceramic coatings on aluminum components, including hard anodizing, gas-flame spray, plasma thermal spray, and physical vapour deposition methods [4–8].

The protection of aluminum alloys by applying micro-arc oxidation (MAO) coatings is currently of great interest. With the introduction of hard ceramic coatings by means of micro-arc oxidation, the wear-resistance, corrosion resistance, mechanical strength, and electrical insulation of the metals and their alloys can be effectively increased [9–13]. Previously, many scientists have paid more attention on optimizing parameters [14–18] to obtain high quality MAO Al_2O_3 coatings on aluminum alloys, as well as the tribological properties in air, water and oil [19,20]. In fact, lots of machine parts made of aluminum alloys are performed in various harsh environments such as water, sea, and rain. Therefore, it is of primary importance to study the simultaneous corrosion and wear behavior of MAO Al_2O_3 coatings in stimulant corrosive environments. However, the tribological properties of MAO Al_2O_3 coatings in seawater and rainwater have not yet been studied in detail.

In view of the above, the commonly used aluminum alloy 2024Al is selected as the substrate to be synthesized MAO Al_2O_3 coating. We have performed fretting wear experiments of the MAO Al_2O_3 coating in artificial seawater and rainwater compared with that in the distilled water to study the influence of corrosive medium on the friction behavior and wear mechanism of MAO Al_2O_3 coating.

* Corresponding author. Tel.: +86 517 83559196; fax: +86 517 83559041.
E-mail address: dhy@hyit.edu.cn (Hong-yan Ding).

0301-679X/$ - see front matter © 2009 Elsevier Ltd. All rights reserved.
doi:10.1016/j.triboint.2009.12.022

2. Experimental details

2.1. Materials and MAO coating deposition

The disk specimen ($\varnothing 30\,mm \times 5\,mm$) of aluminum alloy 2024Al (0.50% Si plus Fe, 4.2% Cu, 0.50% Mn, 1.40% Mg, 0.30% Zn, balance Al) was used as the substrate. It was ground to an average surface roughness of $R_a = 1.2 \pm 0.3\,\mu m$ and cleaned with distilled water before they were subjected to an oxidation process.

The electrolytic solution was composed of an aqueous solution of KOH (1 g/L) and Na_2SiO_3 (10 g/L). The temperature of the electrolytic solution was kept below 35 °C. A constant current density 2 A/dm^2 on the specimen's surface was adjusted by voltage control during the oxidation processing.

Al_2O_3 coating was prepared on the 2024Al surface with a micro-arc oxidation equipment (20 kW) consisting of a potential adjustable pulsed DC source, a stainless steel container with a sample-holder as the electrolyte cell, and a stirring & cooling system. The 2024Al specimen was used as the anode and the wall of the stainless steel container was used as the cathode, respectively. The Al_2O_3 coatings were then deposited on the 2024Al specimens for 1 h.

2.2. Immersion corrosion test

An immersion corrosion test was conducted to evaluate the corrosion property of the Al_2O_3 coatings. The artificial seawater with a pH value of 8 and rainwater with a pH value of 6.25 were synthesized in the laboratory, according to the composition presented in Table 1. After being abraded with SiC paper (2000 grit), the 2024Al blocks with Al_2O_3 coatings were put into seawater and rainwater for 168 h at room temperature. They were then ultrasonically cleaned in ethanol and dried for further morphological observation and electrochemical measurement.

2.3. Friction and wear test

All wear experiments were performed using a ball-on-flat reciprocal tribometer (UMT-2, CETR, USA). Commercially available 440C stainless steel ($\varnothing 4$ mm) with hardness of 62 HRC was used as the upper mating ball and kept stationary. The 2024Al alloy block coated with the Al_2O_3 coating was the lower specimen and was mounted on the table. The schematic diagram of the frictional pair is shown in Fig. 1. Prior to each wear test, the steel ball and 2024Al specimen were ultrasonically cleaned in acetone for 10 min and then air-dried. The wear experiments were performed at room temperature in distilled water, artificial seawater, and artificial rainwater with the same concentration as used in the immersion corrosion tests.

Each test was done for 1 h with a reciprocating amplitude of 300 μm imposed by the tribometer. The normal load was in the range of 0.5–2 N, and the sliding frequency varied in the range of 5–20 Hz. The aqueous solution was added to the rubbing zone every 20 min using an injection tube. The friction coefficient was obtained from the tribometer automatically. After completion of the fretting, the specimens were ultrasonically cleaned in acetone. Later, their surface characteristics and electrochemical properties were investigated. Note that three replicate tests were conducted for each specimen.

2.4. Electrochemical test

To illustrate the influence of wear and immersion on corrosion, the MAO Al_2O_3 coating specimens with three different states were electrochemically tested. The specimens consisted of: (a) one sample without corrosion or wear (original sample); (b) one sample that had been immersed in rainwater or seawater for 168 h (after immersion); (c) one sample that had suffered corrosive fretting in rainwater or seawater at the load of 2 N and the frequency of 20 Hz for 1 h (after corrosion wear). Six tests were conducted.

(1) the sample without corrosion or wear was electrochemically tested in seawater;
(2) the sample without corrosion or wear was electrochemically tested in rainwater;
(3) the sample without corrosion or wear was immersed in seawater and was then electrochemically tested;
(4) the sample without corrosion or wear was immersed in rainwater and was then electrochemically tested;
(5) the sample without corrosion or wear underwent fretting in seawater and was then electrochemically tested;
(6) the sample without corrosion or wear underwent fretting in rainwater and was then electrochemically tested.

Electrochemical measurements were carried out at room temperature using a potentiostat/galvanostat system (CHI760B, China) with a three-electrode cell. The specimen was used as the working electrode and the Al_2O_3 coating was the liquid-contact surface. A platinum plate and saturated calomel electrode (SCE) were used as the counter and reference electrodes, respectively.

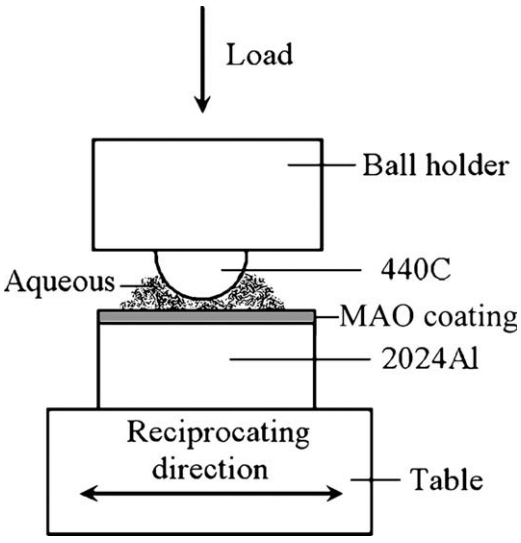

Fig. 1. Schematic diagram of the frictional pair.

Table 1
Main chemical composition of corrosion media of artificial rainwater and artificial seawater (mg dm^{-3}).

Media	SO_4^{2-}	Cl^-	NO_3^-	NH_4^+	Na^+	K^+	Mg^{2+}	Ca^{2+}	SiO_3^{2-}	PO_4^{3-}	CO_3^-
Artificial rainwater	34.18	2.68	4.01	1.57	1.55	1.08	2.08	9.72	–	–	–
Artificial seawater	2.71	19.34	–	–	10.73	0.40	1.29	0.41	0.03	0.03	0.2

A dynamic scan at a potential scanning rate of 0.1 mV/s was performed in corresponding seawater and rainwater according to the solution in which it immersed or worn before. Potentiodynamic anodic polarization curves were automatically acquired. The corrosion potential (E_{corr}) and corrosion current density (i_{corr}) were calculated by software using the *Tafel extrapolation method*.

2.5. Characterization

The thickness of the MAO Al_2O_3 coating was measured on a MINITEST 1100 coating thickness gauge (Elektro-physik Koln, Germany) based on the eddy current technique. The micro-hardness of the MAO Al_2O_3 coating was measured at 4.9 N for 10 s by a digital micro-hardness tester (HXD-1000TM, China) and repeated for 5 times. The structure of the MAO Al_2O_3 coating was determined by D8-Advance X-ray diffraction (XRD) (Bruker, Germany).

The morphology of the corrosive surface and wear scar was observed using a HITACHI 3000N scanning electron microscope (SEM). The chemical composition of the wear scar was investigated with a PHI-5702 multi-functional X-ray photoelectron spectroscope (XPS) having Al K_α radiation as the excitation source and the binding energy of contaminated carbon (C_{1s} at 284.8 eV) as the reference. The 3D-morphology, the profile across the center and the wear volume-loss were investigated using a Micro-XAM non-contact optical profilometer (ADE, USA).

3. Results

3.1. Microstructure, thickness, and micro-hardness of MAO Al_2O_3 coating

Fig. 2 shows the SEM surface micrograph of the MAO coating on 2024Al substrate. The Al_2O_3 coating is porous and loose, with a large number of lamellar spherical pieces like volcano top disorderly arrayed on the surface. Some micro-cracks appear on the coating surface, which could be initiated by the thermal stress attributed to the rapid solidification of the alumina melted in the discharge tunnel.

The XRD pattern of the Al_2O_3 coating after polishing is shown in Fig. 3. It can be seen that the MAO Al_2O_3 coating consists mainly of α-Al_2O_3 and γ-Al_2O_3. It is believed that α-Al_2O_3 phase is thermodynamically stable at all temperature, whereas γ-Al_2O_3 phase is metastable. Ref. [13] reported that α-Al_2O_3 content continuously increases towards the coating/substrate interface due to the cooling rate difference between outlayer region and internal region. Because the mechanical property of α-Al_2O_3 phase is better than that of γ-Al_2O_3 phase, the hardness of internal region is higher than that of outlayer region. The surface subjected to the wear is about 1148 HV in hardness. In the present work the

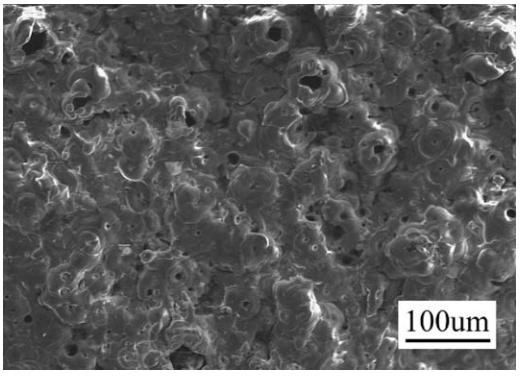

Fig. 2. SEM photograph of the MAO coating.

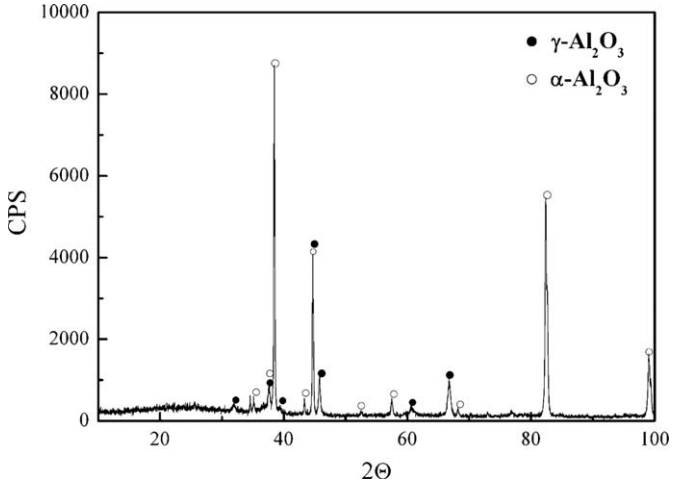

Fig. 3. XRD spectrum of the MAO coating after polishing.

MAO Al_2O_3 coating is abraded with SiC paper within 67 μm thickness to remove the outer loose layer; the 3D-image of the polished surface is illustrated in Fig. 4.

3.2. Corrosion properties of MAO Al_2O_3 coating in artificial rainwater and seawater

The corrosion images of MAO Al_2O_3 coatings' surface after 168 h of immersion in rainwater and seawater are given in Fig. 5. They are slightly different from those in Fig. 2, but the holes in seawater are larger than that in rainwater. Some corrosion holes can be observed on both the surfaces. This implies a better corrosion resistance in rainwater.

3.3. Friction behavior of MAO Al_2O_3 coatings in various aqueous environments

The friction coefficient of the MAO Al_2O_3 coating sliding against the 440C stainless steel ball in distilled water, artificial seawater, and artificial rainwater at various normal loads and frequencies are illustrated in Fig. 6. It is clear that the friction coefficient decreases with an increase of the frequency from 5 to 20 Hz in all the three aqueous solutions, among which the variation in seawater is the smoothest, as shown in Fig. 6(a).

From Fig. 6(b) one can see that the friction coefficient presents different variation trends in three aqueous environments when the normal load increases from 0.5 to 2 N at 20 Hz. With the increasing of the normal load, the friction coefficient decreases slightly in distilled water and increases slightly in seawater, whereas the friction coefficient increases firstly and then decreases in rainwater. The variation of the friction coefficient versus load in seawater is still the smoothest.

It is worth noticing that the friction coefficient is always the highest in rainwater and the lowest in seawater. It decreases about 47% in seawater compared with that in distilled water. This indicates that the aqueous environment does play a considerable influence on the friction coefficient, and the remarkable antifriction effect of the seawater is of particular note.

In the case of the load of 2 N, the frequency dependence of the wear volume-loss in the three aqueous solutions is shown in Fig. 7. It is evident that all the wear volume-loss increases with an increase in frequency. When fretting occurred at low frequency of 5 Hz, the wear-loss in distilled water was always found to be the highest, that is, wear-loss in both the corrosive environments was lower than that in distilled water. This result indicates that a

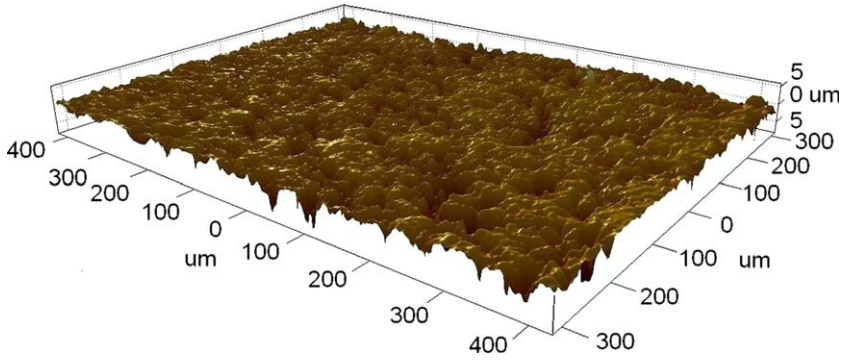

Fig. 4. 3D-image of the MAO coating after polishing.

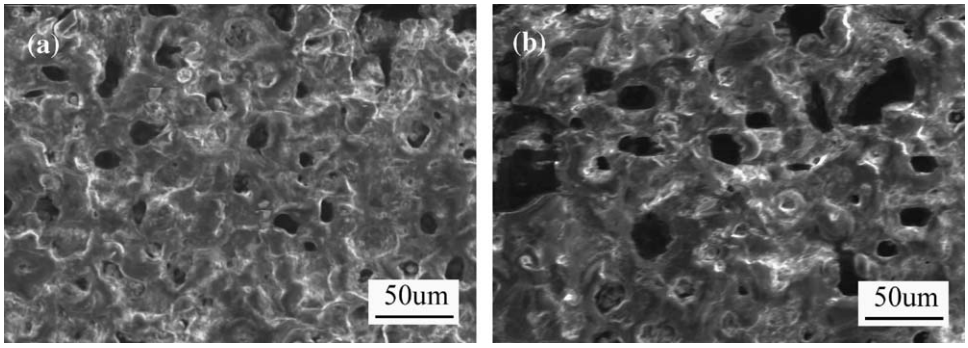

Fig. 5. SEM photographs of MAO Al_2O_3 coating after immersing in rainwater and seawater: (a) in rainwater; (b) in seawater.

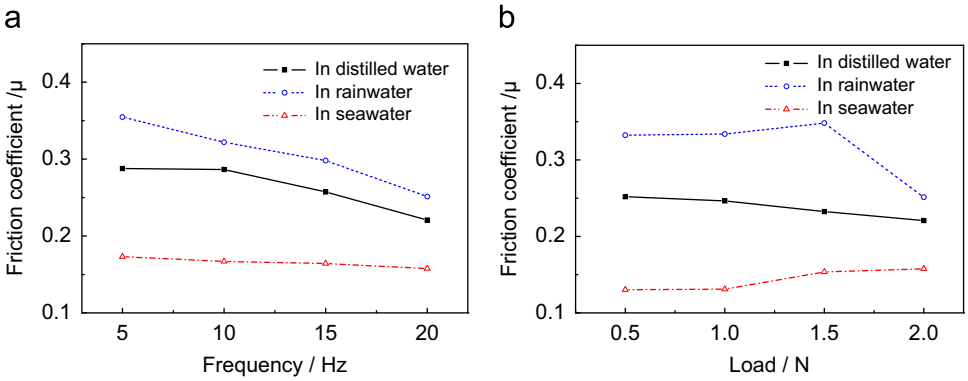

Fig. 6. Friction coefficient in various environments: (a) the frequency versus friction coefficient at the load of 2 N; (b) the load versus friction coefficient at the frequency of 20 Hz.

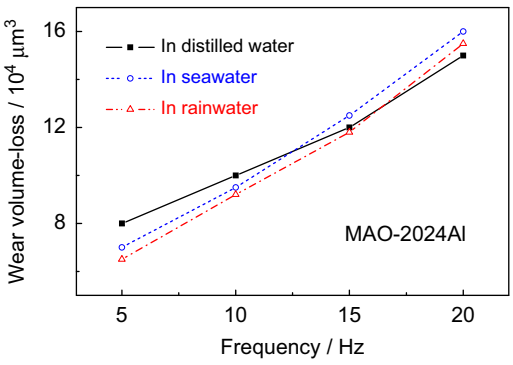

Fig. 7. Wear-loss of the coating under different frequencies at the load of 2 N.

negative synergy ratio between corrosion and wear appears at low frequency. When the frequency increased, the wear-loss increased rapidly in seawater, increased at a slower rate in rainwater, and increased slowest of all in distilled water. The wear-loss in seawater was larger than that in distilled water when the frequency exceeded 10 Hz; the wear-loss in rainwater was larger than that in distilled water when the frequency exceeded 15 Hz; the wear-loss was the greatest in seawater and the lowest in distilled water at the frequency of 20 Hz. Such trend of results strongly suggests that the MAO Al_2O_3 coatings in both the artificial seawater and rainwater present a positive synergy ratio between corrosion and wear at high frequency.

The typical cross-sectional profiles of the wear scars are shown in Fig. 8. All the profile curves present approximate U-shape, among which it is the shallowest and narrowest in distilled water and the deepest and widest in seawater. This also demonstrates

the variation trends of the wear-loss according with the experiment results.

3.4. Electrochemical properties of MAO Al_2O_3 coating in artificial rainwater and seawater

The corrosion potential (E_{corr}) and corrosion current density (i_{corr}) of MAO Al_2O_3 coatings with three different states measured in different solutions are summarized in Table 2. The seawater and rainwater used in the immersion corrosion, electrochemical, and fretting tests had the same concentration.

One should note that specimens in rainwater possess much higher E_{corr} than those in seawater. This indicates that the corrosion tendency in rainwater is less than that in seawater. After an immersion-in-seawater period of 168 h, the E_{corr} of the MAO Al_2O_3 coating decreased by 256 mV and the i_{corr} is reduced to about 1/10 compared with the original sample. However, the E_{corr} and the i_{corr} values showed no significant increment after immersion in rainwater, and the polarization curves of the Al_2O_3 coating before and after immersion were in almost the same shape and position, evidenced in Fig. 9(a).

After fretting in corrosive solutions, both the E_{corr} of Al_2O_3 coating shifted to a negative direction in comparison of the original sample and i_{corr} value in seawater increased almost 2.4 times as much as that of the original sample. Furthermore the i_{corr} in seawater is 6 times as much as that in rainwater. All these resulted from the fact that corrosion resistance considerably decreased after corrosion fretting. It can be concluded that the wear accelerates the corrosion, especially that occurs in seawater.

4. Discussion

4.1. Influence of medium on the friction coefficient

Generally, the friction and wear behavior at contact surface was largely governed by the physical condition of the contacting interface and the chemical interactions between the sliding interfaces and environment [19]. All the wear scars of MAO Al_2O_3 coating in different aqueous solutions present regular concave as the 3D-morphology shown in Fig. 10. One can see that the actual amplitude of sliding is about 400 μm and thus it is impossible for tiny debris to be completely expelled from the wear surface scar due to relative closed contact zone. When the tribo-pair fretting in corrosive solutions of seawater and rainwater, active elements such as S, P, and Cl would react with the element Fe on the surface of the 440C ball [21], and thus an easy-shear-tribo-layer containing ferric sulfide, ferric phosphate, and ferric chloride can be formed. As Ref. [22] pointed out chlorides have a lubricating effect. Furthermore, with the aid of flowing aqueous solution at a certain frequency, the debris wrapped by the lubricative media may act as rolling balls, and thus made the wear process smoother [23]. Therefore, the friction coefficient decreased in the seawater and rainwater compared with distilled water.

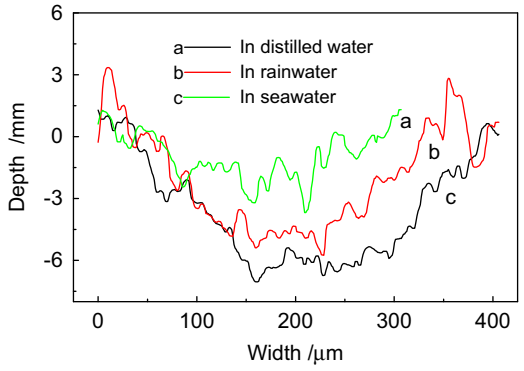

Fig. 8. Profile curves of wear scars in different media at the load of 2 N.

4.2. Influence of medium on the wear-loss

Low frequency means low sliding velocity and less cycle number. The calculation predicts that frequency of 5 and 10 Hz correspond to the cycle number of 3.6×10^4 and 7.2×10^4, and the total sliding distance of 10.8 and 21.6 m. The total sliding distance is so short that the synergism between corrosion and wear does not have enough time to play its role, on the contrary, the friction process gets much smoother because of a lubricating fluid film formed in seawater or rainwater, the antifriction effect thus predominate over the synergism between corrosion and wear. The wear-loss of the MAO Al_2O_3 coating in corrosive solution is accordingly less than that in distilled water when fretting occurs at low frequency. As frequency increases, the sliding speed and sliding distance get improved and the electrochemical effect would be therefore enhanced. The corrosion strongly accelerates the wear under the cooperation of the mechanical and chemical functions; meanwhile, the corrosion speed would increase rapidly due to the surface defects caused by wear, confirmed by electrochemical results mentioned above. As a result, the wear-loss of the MAO Al_2O_3 coating in seawater or rainwater is larger than that in distilled water at high frequency, and leads to a positive synergism between corrosion and wear.

It can be further confirmed by XPS analysis of the MAO Al_2O_3 coating after fretting in rainwater. Cl^- ion was found to be existed in the wear scars of both the corrosive solutions from XPS spectra, as evidenced in Fig. 11.

Possibly the porosity of the MAO is beneficial for Cl^- ion to reside in and thus have more opportunity to erode the matrix material. Since the seawater has higher concentration chloride compared with that of rainwater, the effect of wear accelerating corrosion is more significant (see the electrochemical analysis in Section 3.3). Therefore, the synergy between wear and corrosion of MAO Al_2O_3 coating in seawater is greater than that in rainwater.

Table 2
Results of polarization experiments of MAO Al_2O_3 coating with three different states measured in rainwater and seawater.

Medium	State	Scanning scope/V	Corrosion potential (E_{corr})/V	Corrosion current density (i_{corr})/A
Rainwater	Original sample	−0.5 to 1	−0.011	1.465×10^{-6}
	After immersion	−0.5 to 1	+0.021	1.866×10^{-6}
	After corrosion wear	−1.5 to 1	−0.415	1.010×10^{-6}
Seawater	Original sample	−0.5 to 1	−0.353	1.904×10^{-6}
	After immersion	−0.5 to 1	−0.509	1.654×10^{-7}
	After corrosion wear	−1.5 to 1	−0.593	6.473×10^{-6}

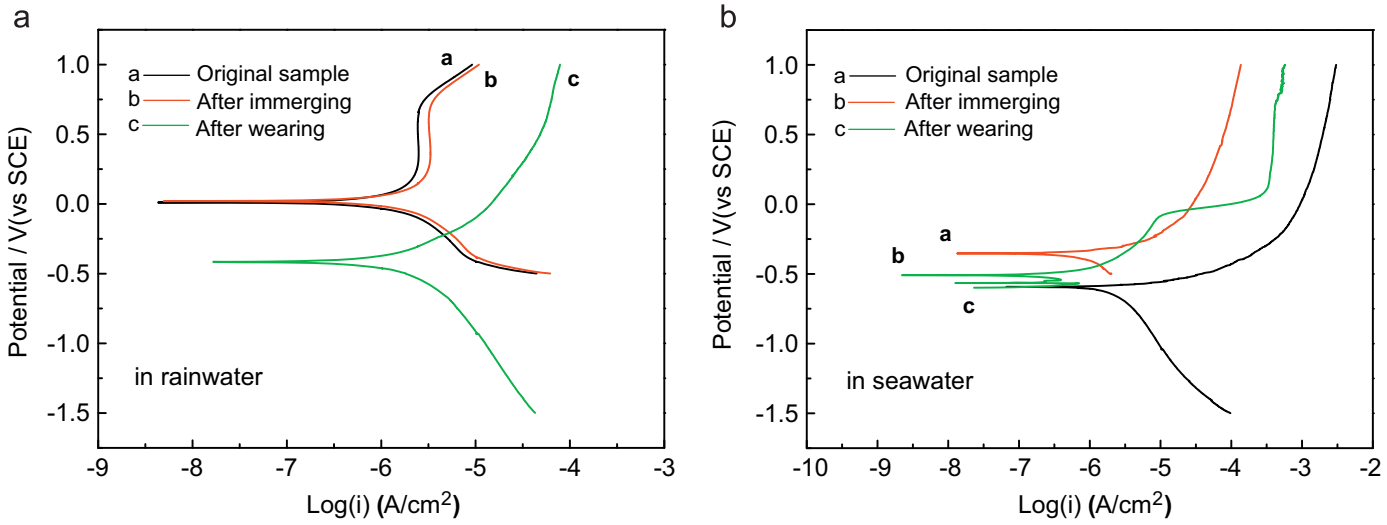

Fig. 9. Polarization curves of MAO Al_2O_3 coatings with three different states: (a) in rainwater; (b) in seawater.

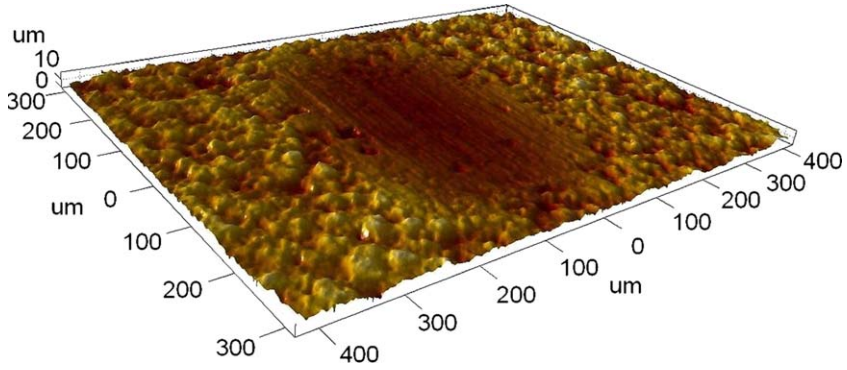

Fig. 10. 3D-morphology of the wear scar.

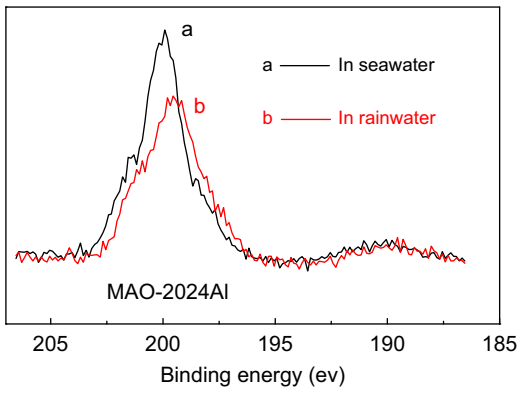

Fig. 11. XPS spectra of the wear scars in corrosion media (Cl_{2p}).

4.3. Wear mechanism

Fig. 12 depicts SEM images of wear scar surfaces in different media after cleaning. It is obvious that the fretting in all the three aqueous solutions induce "smoothing" of the surface by galling the asperities on the porous MAO Al_2O_3 surfaces. Ref. [24] indicated that the tribochemical wear was characterized by a smooth and flat surface and the delamination and dissolution of hydration reaction products; the tribochemical reaction such as hydration reaction between tribo-materials and water during sliding friction period easily occurred. This indicates that the wear debris reacted with water to form lubrication gels such as $Al(OH)_3$ or $Si(OH)_4$ at the contact surface [19]. Thus, the wear mechanism is a coexistence of mechanical wear and tribochemical wear.

One can also see that some scratch lines parallel to the direction of friction with a little spalling pits and micro-cracks were observed in the worn surface of rainwater (see Fig. 12(b)), and some typical corrosive mud was presented in local worn scar of seawater (see Fig. 12(d)). This demonstrates the corrosion effect of higher concentration Cl^- ion on the worn surface. Therefore, the dominant wear mechanism of MAO Al_2O_3 coatings is corrosive delamination fatigue in seawater and that associate with abrasive wear in rainwater.

5. Conclusions

The friction and wear behaviors of the MAO Al_2O_3 coatings against 440C stainless steel ball were investigated in distilled water, artificial seawater, and artificial rainwater at various normal loads and frequencies in fretting contact. The conclusions are summarized as:

(1) MAO Al_2O_3 coating possesses a better corrosion resistance in rainwater than that in seawater.
(2) The friction coefficient decreases with an increase in frequency in all the three aqueous environments of distilled

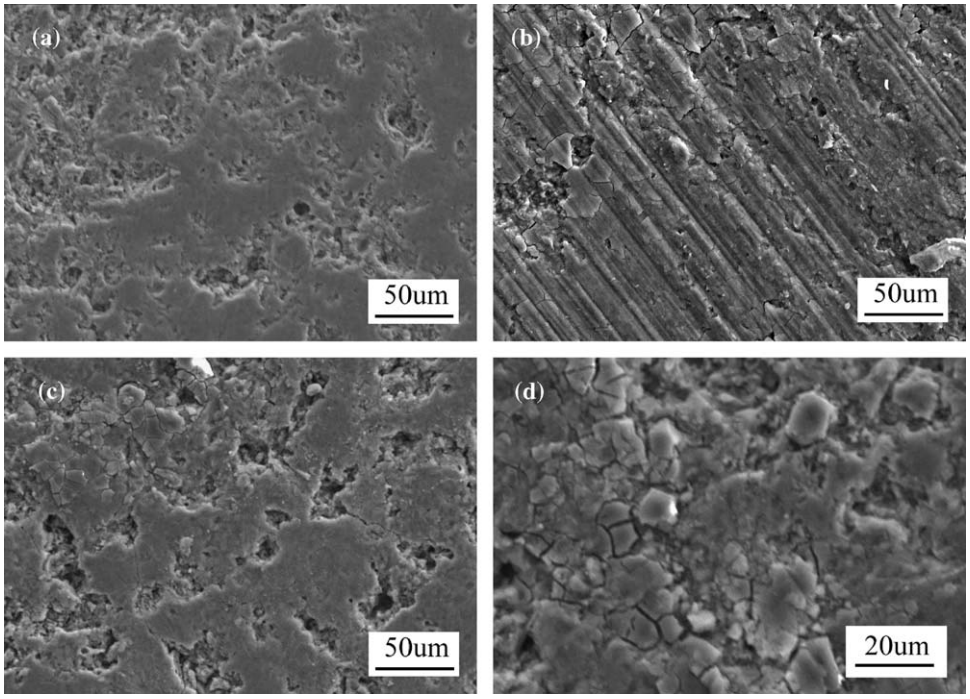

Fig. 12. SEM photographs of wear scars in different media: (a) in distilled water; (b) in rainwater; (c) in seawater; (d) a local worn surface in seawater at a larger amplification.

water, artificial seawater, and artificial rainwater. With an increase in the normal load, the friction coefficient decreases slightly in distilled water and increases slightly in seawater, whereas it increases firstly and then decreases in rainwater.

(3) The friction coefficient is the highest in rainwater and the lowest in seawater at all conditions studied. The aqueous does play a considerable influence on the friction coefficient, the remarkable antifriction effect of the seawater is of particular note.

(4) The wear-loss of the MAO Al_2O_3 coating in distilled water is the highest at low frequency of 5 Hz, which means a negative synergy ratio between corrosion and wear in seawater or rainwater. However, the MAO Al_2O_3 coating presents a positive synergy ratio between corrosion and wear at high frequency.

(5) The fretting in all the three aqueous solutions induce "smoothing" of the surface by galling the asperities on the porous MAO Al_2O_3 surfaces. The dominant wear mechanism of MAO Al_2O_3 coatings is corrosive delamination fatigue in seawater and that associate with abrasive wear in rainwater.

Acknowledgements

This work was supported by Jiangsu key laboratory of friction wear opening foundation under Grant no. kjsmcx07003. The author would like to acknowledge Mr. Tongbo Wei for his help on the preparation of the MAO Al_2O_3 coating.

References

[1] Akarca SS, Altenhof WJ, Alpas AT. Subsurface deformation and damage accumulation in aluminum–silicon alloys subjected to sliding contact. Tribol Int 2007;40(5):735–47.
[2] Elliott III CB, Hoeppner DW. The importance of wear and corrosion on the fretting fatigue behavior of two aluminum alloys. Wear 1999;236:128–33.
[3] Mondal DP, Das S, Prasad BK. Study of erosive–corrosive wear characteristics of an aluminium alloy composite through factorial design of experiments. Wear 1998;217:1–6.
[4] Westergård R, Erickson LC, Axén N, Hawthorne HM, Hogmark S. The erosion and abrasion characteristics of alumina coatings plasma sprayed under different spraying conditions. Tribol Int 1998;31(5):271–9.
[5] Blau Peter J, Walukas Mathew. Sliding friction and wear of magnesium alloy AZ91D produced by two different methods. Tribol Int 2000;33(8):573–9.
[6] Majzoobi GH, Nemati J, Novin Rooz AJ, Farrahi GH. Modification of fretting fatigue behavior of Al7075–T6 alloy by the application of titanium coating using IBED technique and shot peening. Tribol Int 2009;42(1):121–9.
[7] Abu-Zeid OA, Bates RI. Friction and corrosion resistance of sputter deposited supersaturated metastable aluminium–molybdenum alloys. Surf Coat Technol 1996;86–87:526–9.
[8] Ouyang JH, Sasaki S. Tribological characteristics of low-pressure plasma-sprayed $A1_2O_3$ coating from room temperature to 800 °C. Tribol Int 2005;38(1):49–57.
[9] Wei Tongbo, Yan Fengyuan, Tian Jun. Characterization and wear- and corrosion-resistance of microarc oxidation ceramic coatings on aluminum alloy. J Alloys Compd 2005;389:169–76.
[10] Nie Xie, Meletis EI, Jiang JC, Leyland A, Yerokhin AL, Matthews A. Abrasive wear corrosion properties and TEM analysis of Al_2O_3 coatings fabricated using plasma electrolysis. Surf Coat Technol 2002;149:245–51.
[11] Dearnley PA, Gummersbach J, Weiss H, Ogwu AA, Davies TJ. The sliding wear resistance and frictional characteristics of surface modified aluminium alloys under extreme pressure. Wear 1999;225–229:127–34.
[12] Nie X, Wang L, Konca E, Alpas AT. Tribological behaviour of oxide/graphite composite coatings deposited using electrolytic plasma process. Surf Coat Technol 2004;188–189:207–13.
[13] Tian Jun, Luo Zhuangzi, Qi Shangkui, et al. Structure and antiwear behavior of micro-arc oxidized coatings on aluminum alloy structure and antiwear behavior of micro-arc oxidized coatings on aluminum alloy. Surf Coat Technol 2002;54:1–7.
[14] Wu Hanhua, Wang Jianbo, Long Beiyu, et al. Ultra-hard ceramic coatings fabricated through microarc oxidation on aluminium alloy. Appl Surf Sci 2005;252:1545–52.
[15] Xin Shi-Gang, Song Li-Xin, Zhao Rong-Gen, Hu Xing-Fang. Properties of aluminium oxide coating on aluminium alloy produced by micro-arc oxidation. Surf Coat Technol 2005;199:184–8.
[16] Song Xigui, Bian Xiufang, Qi Xiaogang, Zhang Junyan. Fabrication of ceramic layer on an Al–Si alloy by MAO process. Rare Met 2003;22(2):103–6.
[17] Snizhko LO, Yerokhin AL, Pilkington A, Gurevina NL, Misnyankin DO, Leyland A, et al. Anodic processes in plasma electrolytic oxidation of aluminium in alkaline solutions. Electrochim Acta 2004;49:2085–95.
[18] Zheng HY, Wang YK, Li BS, Han GR. The effects of Na_2WO_4 concentration on the properties of microarc oxidation coatings on aluminum alloy. Mater Lett 2005;9:139–42.
[19] Zhou F, Wang Y, Ding H, et al. Friction characteristic of micro-arc oxidative Al_2O_3 coatings sliding against Si_3N_4 balls in various environments. Surf Coat Technol 2008;202:3808–14.
[20] Lukiyanchuk IV, Rudnev VS, Kuryavyi VG, Boguta DL, Bulanova SB, Gordienko PS. Surface morphology, composition and thermal behavior of tungsten

containing anodic spark coatings on aluminium alloy. Thin Solid Films 2004;446:54–60.
[21] Ding HY, Dai ZD, Zhou F, Zhou GH. Sliding friction and wear behavior of TC11 in aqueous condition. Wear 2007;263:117–24.
[22] Hanawa T, Asami K, Asaoka K. Repassivation of titanium and surface oxide film regeneration in simulated bioliquid. J Biomed Mater Res 1998;40:530–8.
[23] Neville A, Morina A, Haque T, Voong M. Compatibility between tribological surfaces and lubricant additives—How friction and wear reduction can be controlled by surface/lube synergies. Tribol Int 2007;40:1680–95.
[24] Fischer TE, Mullins WM. Chemical aspects of ceramic tribology. J Phys Chem 1992;96:5690.